

## Diversity of New Structural Types in Polynuclear Iron Chemistry with a Tridentate N,N,O Ligand

Rashmi Bagai,<sup>†</sup> Saiti Datta,<sup>‡</sup> Amalia Betancur-Rodriguez,<sup>‡</sup> Khalil A. Abboud,<sup>†</sup> Stephen Hill,<sup>‡</sup> and George Christou<sup>\*,†</sup>

Department of Chemistry and Department of Physics, University of Florida, Gainesville, Florida 32611-7200

Received January 21, 2007

The syntheses, crystal structures, and magnetochemical characterization of four new iron clusters  $[\text{Fe}_7\text{O}_4(\text{O}_2\text{CPh})_{11}(\text{dmem})_2]$  (**1**),  $[\text{Fe}_7\text{O}_4(\text{O}_2\text{CMe})_{11}(\text{dmem})_2]$  (**2**),  $[\text{Fe}_6\text{O}_2(\text{OH})_4(\text{O}_2\text{CBu}^t)_8(\text{dmem})_2]$  (**3**), and  $[\text{Fe}_3\text{O}(\text{O}_2\text{CBu}^t)_2(\text{N}_3)_3(\text{dmem})_2]$  (**4**) ( $\text{dmemH} = \text{Me}_2\text{NCH}_2\text{CH}_2\text{N}(\text{Me})\text{CH}_2\text{CH}_2\text{OH}$ ) = 2-[2-(dimethylamino)ethyl]methylamino}ethanol) are reported. The reaction of **dmemH** with  $[\text{Fe}_3\text{O}(\text{O}_2\text{CR})_6(\text{H}_2\text{O})_3](\text{NO}_3)$  ( $\text{R} = \text{Ph}$  (**1**),  $\text{Me}$  (**2**), and  $\text{Bu}^t$  (**3**)) gave **1**, **2**, and **3**, respectively, whereas **4** was obtained from the reaction of **3** with sodium azide. The complexes all possess rare or novel core topologies. The core of **1** comprises two  $[\text{Fe}_4(\mu_3\text{-O})_2]^{8+}$  butterfly units sharing a common body Fe atom. The core of **2** consists of a  $[\text{Fe}_3\text{O}_3]$  ring with each doubly bridging  $\text{O}^{2-}$  ion becoming  $\mu_3$  by also bridging to a third, external Fe atom; a seventh Fe atom is attached on the outside of this core via an additional  $\mu_3\text{-O}^{2-}$  ion. The core of **3** consists of a  $[\text{Fe}_4(\mu_3\text{-O})_2]^{8+}$  butterfly unit with an Fe atom attached above and below this by bridging O atoms. Finally, the core of **4** is an isosceles triangle bridged by a  $\mu_3\text{-O}^{2-}$  ion with a rare T-shaped geometry and with the azide groups all bound terminally. Variable-temperature, solid-state dc, and ac magnetization studies were carried out on complexes **1–4** in the 5.0–300 K range. Fitting of the obtained magnetization ( $M$ ) vs field ( $H$ ) and temperature ( $T$ ) data by matrix diagonalization and including only axial anisotropy (zero-field splitting) established that **1**, **2**, and **4** each possess an  $S = 5/2$  ground state spin, whereas **3** has an  $S = 5$  ground state. As is usually the case, good fits of the magnetization data could be obtained with both positive and negative  $D$  values. To obtain more accurate values and to determine the sign of  $D$ , high-frequency EPR studies were carried out on single crystals of representative complexes **1**·4MeCN and **3**·2MeCN, and these gave  $D = +0.62 \text{ cm}^{-1}$  and  $|E| \geq 0.067 \text{ cm}^{-1}$  for **1**·4MeCN and  $D = -0.25 \text{ cm}^{-1}$  for **3**·2MeCN. The magnetic susceptibility data for **4** were fit to the theoretical  $\chi_M$  vs  $T$  expression derived by the use of an isotropic Heisenberg spin Hamiltonian and the Van Vleck equation, and this revealed the pairwise exchange parameters to be antiferromagnetic with values of  $J_a = -3.6 \text{ cm}^{-1}$  and  $J_b = -45.9 \text{ cm}^{-1}$ . The combined results demonstrate the ligating flexibility of **dmem** and its usefulness in the synthesis of a variety of  $\text{Fe}_x$  molecular species.

### Introduction

Polynuclear iron compounds with oxygen-based ligation are relevant to a variety of fields such as bioinorganic chemistry and magnetic materials. Iron–oxo centers are found in several non-heme metalloproteins and metalloenzymes; for example, in mammals, iron is stored as ferritin, a protein that sequesters iron(III) as a polymeric oxo-hydroxo

complex.<sup>1</sup> A number of polynuclear iron complexes have thus been synthesized and studied as possible models for ferritin to gain insights into the biomineralization process involved in the formation of its metal core.<sup>2</sup> On the other hand, the paramagnetic nature of Fe in its common oxidation states can often lead to interesting magnetic properties for

\* To whom correspondence should be addressed. E-mail: christou@chem.ufl.edu. Tel: +1-352-392-8314. Fax: +1-352-392-8757.

<sup>†</sup> Department of Chemistry.

<sup>‡</sup> Department of Physics.

(1) Bertini, I.; Gray, H. B.; Lippard, S. J.; Valentine, J. S. *Bioinorganic Chemistry*; University Science Books: Mill Valley, CA, 1994.

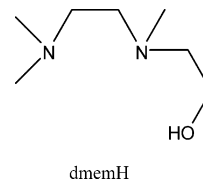
(2) (a) Goodwin, J. C.; Sessoli, R.; Gatteschi, D.; Wernsdorfer, W.; Powell, Annie, K.; Heath, S. L. *Dalton* **2000**, 12, 1835–1840. (b) Gorun, S. M.; Papaefthymiou, G. C.; Frankel, R. B.; Lippard, S. J. *J. Am. Chem. Soc.* **1987**, 109, 4244–4255. (c) Taft, K. L.; Papaefthymiou, G. C.; Lippard, S. J. *Science* **1993**, 259, 1302–1305.

polynuclear Fe clusters, such as high ground-state spin values and even single-molecule magnetism.<sup>3</sup>

Although the exchange interactions between Fe(III) centers are almost always antiferromagnetic, certain Fe<sub>x</sub> topologies can nevertheless possess large ground-state spin values as a result of spin frustration. The latter is here defined in its more general sense of competing exchange interactions of comparable magnitude, preventing (frustrating) the preferred antiparallel alignment of all spins, and thus giving larger ground-state spin values than might be predicted.<sup>4</sup> In favorable cases, where these large ground-state spins are coupled to a significant magnetic anisotropy, the compounds can behave as single-molecule magnets (SMMs).<sup>5</sup> This is the case for SMMs such as [Fe<sub>8</sub>O<sub>2</sub>(OH)<sub>12</sub>(tacn)<sub>6</sub>]<sup>8+</sup>, [Fe<sub>4</sub>(OMe)<sub>6</sub>(dpm)<sub>6</sub>], etc.<sup>6</sup>

The above considerations and others continue to stimulate groups around the world to develop new synthetic methods that can yield new polynuclear Fe–O clusters. A common approach has been to use chelates to encourage aggregation while ensuring discrete products. Examples include 2,2'-bipyridine (bpy),<sup>7</sup> 1,4,7-triazacyclononane (tacn),<sup>6c</sup> and the anion of dibenzoylmethane (dbm<sup>-</sup>).<sup>8</sup> When the chelate also contains potentially bridging groups such as alkoxides, new high-nuclearity products can be obtained. Examples of this include the deprotonated, tridentate N,O,O form of *N*-methyl-diethanolamine (mdaH<sub>2</sub>) and the O,O,O form of tris-(hydroxymethyl)ethane (thmeH<sub>3</sub>), and others.<sup>9</sup> We recently decided to extend this approach to the potentially tridentate N,N,O chelate 2-[[2-(dimethylamino)ethyl]methylamino]-

ethanol (dmemH). This has some similarity to mdaH<sub>2</sub>, but it only has one alcohol group and it was thus anticipated to



give new structural types of products. We were unable to locate previous examples in the literature of transition-metal complexes with this chelate.

Our first investigations with dmemH have been in Fe chemistry using the triangular [Fe<sub>3</sub>O(O<sub>2</sub>CR)<sub>6</sub>(L)<sub>3</sub>]<sup>+</sup> complexes as reagents, a common strategy in both Fe(III)<sup>10</sup> and Mn(III)<sup>11</sup> chemistry. We have found from these reactions that dmemH is indeed a good route to a variety of interesting new cluster types. These results are described in this paper, which reports the syntheses, structures, and magnetochemical characterization of four new Fe clusters containing dmem<sup>-</sup>.

## Experimental Section

**Syntheses.** All preparations were performed under aerobic conditions using reagents and solvents as received. [Fe<sub>3</sub>O(O<sub>2</sub>CBu)<sub>6</sub>(H<sub>2</sub>O)<sub>3</sub>](NO<sub>3</sub>), [Fe<sub>3</sub>O(O<sub>2</sub>CPh)<sub>6</sub>(H<sub>2</sub>O)<sub>3</sub>](NO<sub>3</sub>), [Fe<sub>3</sub>O(O<sub>2</sub>CMe)<sub>6</sub>(H<sub>2</sub>O)<sub>3</sub>](NO<sub>3</sub>),<sup>12</sup> and (NEt<sub>4</sub>)<sub>2</sub>(Fe<sub>2</sub>OCl<sub>6</sub>)<sup>13</sup> were synthesized as reported elsewhere.

**[Fe<sub>7</sub>O<sub>4</sub>(O<sub>2</sub>CPh)<sub>11</sub>(dmem)<sub>2</sub>] (1). Method A.** An orange-red solution of [Fe<sub>3</sub>O(O<sub>2</sub>CPh)<sub>6</sub>(H<sub>2</sub>O)<sub>3</sub>](NO<sub>3</sub>) (0.20 g, 0.19 mmol) in MeCN (20 mL) was treated with dmemH (0.06 mL, 0.38 mmol), and the solution was stirred overnight at room temperature. It was then filtered to remove undissolved starting material, and the filtrate was allowed to stand undisturbed at room temperature. X-ray-quality orange crystals of 1·4MeCN slowly formed over 5 days in 45% yield. These were collected by filtration, washed with MeCN, and dried under vacuum. Anal. Calcd (found) for 1·½MeCN (C<sub>92</sub>H<sub>90.5</sub>N<sub>4.5</sub>Fe<sub>7</sub>O<sub>28</sub>): C, 52.66 (52.55); H, 4.35 (4.38); N, 3.00 (3.05). Selected IR data (cm<sup>-1</sup>): 1598(m), 1567(m), 1539(m), 1413(vs), 1175(w), 1069(w), 1025(w), 717(m), 675(w), 644(m), 461(m).

**Method B.** A solution of FeCl<sub>3</sub>·6H<sub>2</sub>O (0.20 g, 0.74 mmol) and NaO<sub>2</sub>CPh (0.21 g, 1.48 mmol) in MeCN (15 mL) was treated with dmemH (0.06 mL, 0.37 mmol) and stirred for 3 h. The resultant red-brown solution was filtered to remove NaCl, and the filtrate was left undisturbed at room temperature for slow evaporation.

(3) Christou, G.; Gatteschi, D.; Hendrickson, D. N.; Sessoli, R. *MRS Bull.* **2000**, *25*, 66.

(4) (a) Jones, L. F.; Brechin, E. K.; Collison, D.; Helliwell, M.; Mallah, T.; Piligkos, S.; Rajaraman, G.; Wernsdorfer, W. *Inorg. Chem.* **2003**, *42*, 6601–6603. (b) Powell, A. K.; Heath, S. L.; Gatteschi, D.; Pardi, L.; Sessoli, R.; Spina, G.; Del Giallo, F.; Pieralli, F. *J. Am. Chem. Soc.* **1995**, *117*, 2491–2502. (c) Cañada-Vilalta, C.; O'Brien, T. A.; Brechin, E. K.; Pink, M.; Davidson, E. R.; Christou, G. *Inorg. Chem.* **2004**, *43*, 5505–5521. (d) McCusker, J. K.; Vincent, J. B.; Schmitt, E. A.; Mino, M. L.; Shin, K.; Coggin, D. K.; Hagen, P. M.; Huffman, J. C.; Christou, G.; Hendrickson, D. N. *J. Am. Chem. Soc.* **1991**, *113*, 3012–3021. (e) Kahn, O. *Chem. Phys. Lett.* **1997**, *265*, 109.

(5) Gatteschi, D.; Sessoli, R.; Cornia, A. *Chem. Commun.* **2000**, *9*, 725–732.

(6) (a) Barra, A. L.; Caneschi, A.; Cornia, A.; de Biani, F. F.; Gatteschi, D.; Sangregorio, C.; Sessoli, R.; Sorace, L. *J. Am. Chem. Soc.* **1999**, *121*, 5302–5310. (b) Powell, G. W.; Lancashire, H. N.; Brechin, E. K.; Collison, D.; Health, S. L.; Mallah, T.; Wernsdorfer, W. *Angew. Chem., Int. Ed.* **2004**, *43*, 5772–5775. (c) Delfs, C.; Gatteschi, D.; Pardi, L.; Sessoli, R.; Wieghardt, K.; Hanke, D. *Inorg. Chem.* **1993**, *32*, 3099–3103. (d) Sangregorio, C.; Olin, T.; Paulsen, C.; Sessoli, R.; Gatteschi, D. *Phys. Rev. Lett.* **1997**, *78*, 4645.

(7) McCusker, J. K.; Vincent, J. B.; Schmitt, E. A.; Mino, M. L.; Shin, K.; Coggin, D. K.; Hagen, P. M.; Huffman, J. C.; Christou, G.; Hendrickson, D. N. *J. Am. Chem. Soc.* **1991**, *113*, 3012–3021.

(8) Caneschi, A.; Cornia, A.; Lippard, S. J. *Angew. Chem., Int. Ed.* **1995**, *34*, 467–469.

(9) (a) Murugesu, M.; Abboud, K. A.; Christou, G. *Dalton Trans.* **2003**, *23*, 4552–4556. (b) Jones, L. F.; Batsanov, A.; Brechin, E. K.; Collison, D.; Helliwell, M.; Mallah, T.; McInnes, E. J. L.; Piligkos, S. *Angew. Chem., Int. Ed.* **2002**, *41*, 4318–4321. (c) Moragues-Canovas, M.; Riviere, E.; Ricard, L.; Paulsen, C.; Wernsdorfer, W.; Rajaraman, G.; Brechin, E. K.; Mallah, T. *Adv. Mater.* **2004**, *16*, 1101–1105. (d) Foguet-Albiol, D.; Abboud, K. A.; Christou, G. *Chem. Commun.* **2005**, *34*, 4282–4284. (e) Saalfrank, R. W.; Bernert, I.; Uller, E.; Hampel, F. *Angew. Chem., Int. Ed.* **1997**, *36*, 2482–2485. (e) King, P.; Stamatatos, T. C.; Abboud, K. A.; Christou, G. *Angew. Chem., Int. Ed.* **2006**, *45*, 7379–7383.

(10) (a) Ammala, P.; Cashion, J. D.; Kepert, C. M.; Moubaraki, B.; Murray, K. S.; Spiccia, L.; West, B. O. *Angew. Chem., Int. Ed.* **2000**, *39*, 1688–1690. (b) Murugesu, M.; Abboud, K. A.; Christou, G. *Polyhedron* **2004**, *23*, 2779–2788. (c) Taft, K. L.; Lippard, S. J. *J. Am. Chem. Soc.* **1990**, *112*, 9629–9630. (d) Benelli, C.; Parsons, S.; Solan, G. A.; Winpenny, R. E. P. *Angew. Chem., Int. Ed.* **1996**, *35*, 1825–1828.

(11) (a) Brechin, E. K.; Boskovic, C.; Wernsdorfer, W.; Yoo, J.; Yamaguchi, A.; Sanudo, E. C.; Concolino, T. R.; Rheingold, A. L.; Ishimoto, H.; Hendrickson, D. N.; Christou, G. *J. Am. Chem. Soc.* **2002**, *124*, 9710–9711. (b) Libby, E.; McCusker, J. K.; Schmitt, E. A.; Folting, K.; Hendrickson, D. N.; Christou, G. *Inorg. Chem.* **1991**, *30*, 3486–3495. (c) Vincent, J. B.; Christmas, C.; Chang, H. R.; Li, Q.; Boyd, P. D. W.; Huffman, J. C.; Hendrickson, D. N.; Christou, G. *J. Am. Chem. Soc.* **1989**, *111*, 2086–2097.

(12) (a) Duncan, J. F.; Kanekar, C. R.; Mok, K. F. *J. Chem. Soc. A* **1969**, *3*, 480–482. (b) Earnshaw, A.; Figgis, B. N.; Lewis, J. *J. Chem. Soc. A* **1966**, *12*, 1656–1663. (c) Bond, A. M.; Clark, R. J. H.; Humphrey, D. G.; Panayiotopoulos, P.; Skelton, B. W.; White, A. H. *J. Chem. Soc., Dalton Trans.* **1998**, *11*, 1845–1852.

(13) Armstrong, W. H.; Lippard, S. J. *Inorg. Chem.* **1985**, *24*, 981–982.

Orange crystals slowly formed over 5 days in 30% yield; the product was identified by IR spectral comparison with material from method A.

**Method C.** A solution of  $(\text{NEt}_4)_2(\text{Fe}_2\text{OCl}_6)$  (0.20 g, 0.33 mmol) and  $\text{NaO}_2\text{CPh}$  (0.14 g, 0.99 mmol) in MeCN (15 mL) was treated with dmemH (0.11 mL, 0.66 mmol) and stirred for a few hours. The resultant red-brown solution was filtered and kept undisturbed at room temperature for slow evaporation. Orange crystals slowly formed over 3 days in 40% yield; the product was identified by IR spectral comparison with material from method A.

**[Fe<sub>3</sub>O<sub>4</sub>(O<sub>2</sub>CMe)<sub>11</sub>(dmem)<sub>2</sub>] (2).** **Method A.** A solution of  $\text{FeCl}_3 \cdot 6\text{H}_2\text{O}$  (0.20 g, 0.74 mmol) and  $\text{NaO}_2\text{CMe} \cdot 3\text{H}_2\text{O}$  (0.25 g, 1.85 mmol) in MeCN (15 mL) was treated with dmemH (0.06 mL, 0.37 mmol) and stirred for 3 h. The resultant red-brown solution was filtered to remove NaCl, and the filtrate was left undisturbed at room temperature for slow evaporation. X-ray-quality dark-orange crystals appeared over 20 days in 15% yield. These were collected by filtration, washed with MeCN, and dried under vacuum. Anal. Calcd (found) for **2**·2MeCN ( $\text{C}_{40}\text{H}_{73}\text{N}_6\text{Fe}_7\text{O}_{28}$ ): C, 32.53 (32.66); H, 4.98 (5.26); N, 5.69 (5.46). Selected IR data ( $\text{cm}^{-1}$ ): 3431(br), 2985(w), 2875(w), 1565(vs), 1426(vs), 1088(w), 1052(w), 1033(w), 886(w), 709(w), 668(m), 637(m), 615(m), 539(m), 487(m).

**Method B.** An orange-red solution of  $[\text{Fe}_3\text{O}(\text{O}_2\text{CMe})_6(\text{H}_2\text{O})_3](\text{NO}_3)$  (0.20 g, 0.03 mmol) in MeCN (15 mL) was treated with dmemH (0.10 mL, 0.06 mmol), and the solution was stirred overnight at room temperature. It was then filtered, and the filtrate was allowed to stand undisturbed at room temperature. Orange crystals of the product formed over 25 days in 10% yield; the product was identified by IR spectral comparison with material from method A.

**[Fe<sub>6</sub>O<sub>2</sub>(OH)<sub>4</sub>(O<sub>2</sub>CCBu<sup>t</sup>)<sub>8</sub>(dmem)<sub>2</sub>] (3).** A solution of dmemH (0.03 mL, 0.19 mmol) in MeCN (5 mL) was treated with pyridine (15  $\mu\text{L}$ , 0.19 mmol), followed by the addition of a solution of  $[\text{Fe}_3\text{O}(\text{O}_2\text{CBu}^t)_6(\text{H}_2\text{O})_3](\text{NO}_3)$  (0.18 g, 0.19 mmol) in MeCN (12 mL). The resultant solution was filtered, and the filtrate was left undisturbed at room temperature. X-ray-quality orange needles of **3**·2MeCN grew over 10 days in 20% yield. These were collected by filtration, washed with MeCN, and dried under vacuum. The dried solid was analyzed as solvent-free. Anal. Calcd (found) for **3** ( $\text{C}_{54}\text{H}_{110}\text{N}_4\text{Fe}_6\text{O}_{24}$ ): C, 42.27 (42.53); H, 7.23 (7.40); N, 3.65 (3.68). Selected IR data ( $\text{cm}^{-1}$ ): 2960(m), 2925(w), 2866(w), 1558(vs), 1484(s), 1427(vs), 1376(w), 1332(w), 1228(m), 1073(w), 903(w), 787(w), 662(m), 608(m), 530(m), 427(m).

**[Fe<sub>3</sub>O(O<sub>2</sub>CBu<sup>t</sup>)<sub>2</sub>(N<sub>3</sub>)<sub>3</sub>(dmem)<sub>2</sub>] (4).** A solution of  $[\text{Fe}_3\text{O}(\text{O}_2\text{CBu}^t)_6(\text{H}_2\text{O})_3](\text{NO}_3)$  (0.10 g, 0.11 mmol) in EtOH (15 mL) was treated with dmemH (34  $\mu\text{L}$ , 0.20 mmol) and solid sodium azide (0.03 g, 0.46 mmol) and then stirred overnight at room temperature to give an orange precipitate. The solid was collected by filtration and washed with a little EtOH. It was recrystallized from a  $\text{CH}_2\text{Cl}_2$ /hexanes layering to give X-ray-quality orange crystals of **4**· $\frac{1}{2}\text{CH}_2\text{Cl}_2$  over 3 days in 25% yield. Anal. Calcd (found) for **4**· $\frac{1}{2}\text{CH}_2\text{Cl}_2$  ( $\text{C}_{24.5}\text{H}_{53}\text{N}_{13}\text{Fe}_3\text{O}_7\text{Cl}$ ): C, 34.83 (34.77); H, 6.32 (6.30); N, 21.55 (21.16). Selected IR data ( $\text{cm}^{-1}$ ): 3390(br), 2959(w), 2870(w), 2066(vs), 1543(m), 1480(w), 1418(m), 1342(w), 1225(w), 1087(m), 986(w), 720(m), 633(w), 606(w), 429(w).

**X-ray Crystallography.** Data were collected on a Siemens SMART PLATFORM equipped with a CCD area detector and a graphite monochromator utilizing Mo K $\alpha$  radiation ( $\lambda = 0.71073$  Å). Suitable crystals of **1**·4MeCN, **2**·MeCN, **3**·2MeCN, and **4**· $\frac{1}{2}\text{CH}_2\text{Cl}_2$  were attached to glass fibers using silicone grease and transferred to a goniostat, where they were cooled to 173 K for data collection. Cell parameters were refined using up to 8192 reflections. A full sphere of data (1850 frames) was collected using

**Table 1.** Crystallographic Data for **1**·4MeCN, **2**·MeCN, **3**·2MeCN, and **4**· $\frac{1}{2}\text{CH}_2\text{Cl}_2$

	1	2	3	4
formula <sup>a</sup>	$\text{C}_{99}\text{H}_{101}\text{Fe}_7\text{N}_8\text{O}_{28}$	$\text{C}_{38}\text{H}_{70}\text{Fe}_7\text{N}_5\text{O}_{28}$	$\text{C}_{58}\text{H}_{116}\text{Fe}_6\text{N}_6\text{O}_{24}$	$\text{C}_{25}\text{H}_{54}\text{Cl}_2\text{Fe}_3\text{N}_{13}\text{O}_7$
fw, g/mol <sup>a</sup>	2241.83	1435.94	1616.67	887.26
space group	<i>C</i> 2/ <i>c</i>	<i>P</i> $\bar{1}$	<i>P</i> $\bar{1}$	<i>P</i> 2 <sub>1</sub> / <i>n</i>
<i>a</i> , Å	18.6028(14)	12.4586(8)	12.9769(10)	12.3260(8)
<i>b</i> , Å	26.8523(14)	13.5495(9)	14.4142(11)	25.3961(17)
<i>c</i> , Å	20.8083(13)	18.690(12)	23.9082(18)	13.1400(9)
$\alpha$ , deg	90	70.636(2)	87.6240(10)	90
$\beta$ , deg	103.879(2)	79.731(2)	88.5620(10)	99.1490(10)
$\gamma$ , deg	90	73.099(2)	66.0920(10)	90
<i>V</i> , Å <sup>3</sup>	10090.9(11)	2836.2(3)	4084.7(5)	4060.9(5)
<i>Z</i>	4	2	2	4
<i>T</i> , K	173(2)	173(2)	173(2)	173(2)
radiation, Å <sup>b</sup>	0.71073	0.71073	0.71073	0.71073
$\rho_{\text{calc}}$ , g/cm <sup>3</sup>	1.476	1.681	1.311	1.451
$\mu$ , mm <sup>-1</sup>	1.058	1.828	1.105	1.244
R1 <sup>c,d</sup>	0.0457	0.0353	0.0415	0.0497
wR2 <sup>e</sup>	0.0899	0.0864	0.1009	0.1023

<sup>a</sup> Including solvate molecules. <sup>b</sup> Graphite monochromator. <sup>c</sup>  $I > 2\sigma(I)$ . <sup>d</sup>  $R1 = \sum(|F_o| - |F_c|)/\sum|F_o|$ . <sup>e</sup>  $wR2 = [\sum[w(F_o^2 - F_c^2)^2]/\sum[w(F_o^2)^2]]^{1/2}$ ,  $w = 1/[\sigma^2(F_o^2) + (ap)^2 + bp]$ , where  $p = [\max(F_o^2, O) + 2F_c^2/3]$ .

the  $\omega$ -scan method (0.3° frame width). The first 50 frames were remeasured at the end of data collection to monitor instrument and crystal stability (maximum correction on *I* was <1%). Absorption corrections by integration were applied based on measured indexed crystal faces. The structure was solved by direct methods in *SHELXL6*<sup>14</sup> and refined using full-matrix least squares. The non-H atoms were treated anisotropically, whereas the hydrogen atoms were calculated in ideal positions and were riding on their respective carbon atoms. Refinement was done using  $F^2$ .

In **1**·4MeCN, the asymmetric unit consists of half the Fe<sub>7</sub> cluster and two MeCN molecules of crystallization. A total of 644 parameters were refined in the final cycle of refinement using 32 986 reflections with  $I > 2\sigma(I)$  to yield R1 and wR2 of 4.57 and 8.99%, respectively. In **2**·MeCN, a total of 721 parameters were refined in the final cycle of refinement using 18 637 reflections with  $I > 2\sigma(I)$  to yield R1 and wR2 of 3.53 and 8.64%, respectively. In **3**·2MeCN, a total of 924 parameters were refined in the final cycle of refinement using 17 808 reflections with  $I > 2\sigma(I)$  to yield R1 and wR2 of 4.15 and 10.0%, respectively. In **4**· $\frac{1}{2}\text{CH}_2\text{Cl}_2$ , the azide ligand at N11 was disordered and it was refined in two positions with the site occupation factors dependently refined. A total of 472 parameters were refined in the final cycle of refinement using 9205 reflections with  $I > 2\sigma(I)$  to yield R1 and wR2 of 4.97 and 10.23%, respectively. Unit cell data and details of the structure refinements for the four complexes are listed in Table 1.

**Other Studies.** Infrared spectra were recorded in the solid state (KBr pellets) on a Nicolet Nexus 670 FTIR spectrometer in the 400–4000  $\text{cm}^{-1}$  range. Elemental analyses (C, H, and N) were performed by the in-house facilities of the University of Florida Chemistry Department. Variable-temperature dc and ac magnetic susceptibility data were collected at the University of Florida using a Quantum Design MPMS-XL SQUID susceptometer equipped with a 7 T magnet and operating in the 1.8–300 K range. Samples were embedded in solid eicosane to prevent torquing. Magnetization vs field and temperature data was fit using the program *MAGNET*. Pascal's constants<sup>15</sup> were used to estimate the diamagnetic correction, which was subtracted from the experimental susceptibility to give the molar paramagnetic susceptibility ( $\chi_M$ ). Double-axis angle-

(14) *SHELXL6*; Bruker-AXS: Madison, WI, 2000.

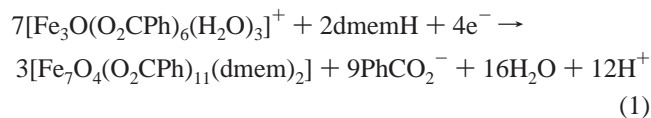
(15) *CRC Handbook of Chemistry and Physics*; Weast, R. C., Ed.; CRC Press, Inc.: Boca Raton, FL, 1984.

dependent high-frequency electron paramagnetic resonance (HFEP) studies were performed on single crystals of **1**·4MeCN and **3**·2MeCN using a rotating cavity<sup>16</sup> and a 7 T transverse magnetic field, which can be rotated about an axis perpendicular to the axis of the rotating cavity. In addition, a 17 T axial magnet was employed for some single-axis measurements. The experiments were carried out over a wide range of frequencies (50–200 GHz) and with the sample at temperatures in the 1.8–20 K range.

## Results and Discussion

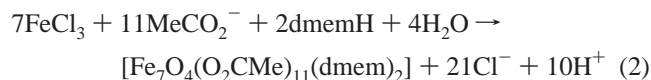
**Syntheses.** Many synthetic procedures to polynuclear iron clusters rely on the reaction of  $[\text{Fe}_3\text{O}(\text{O}_2\text{CR})_6(\text{L})_3]^+$  species with a potentially chelating ligand, and this was one of the procedures chosen in the present work. In such reactions, the  $[\text{Fe}_3\text{O}]^{7+}$  core of the trinuclear iron complex serves as a building block for higher nuclearity species, but the exact nuclearity and structure of the product depend on several factors; in the present work, we have found that the identity of the carboxylate group is one of these.

The reaction of  $[\text{Fe}_3\text{O}(\text{O}_2\text{CPh})_6(\text{H}_2\text{O})_3]^+$  with 1–3 equiv of dmemH in MeCN gave the heptanuclear complex  $[\text{Fe}_7\text{O}_4(\text{O}_2\text{CPh})_{11}(\text{dmem})_2]$  (**1**) with a core topology not previously encountered (eq 1). The same product was obtained from an EtOH reaction solvent and also from the



treatment of an MeCN solution of  $\text{FeCl}_3 \cdot 6\text{H}_2\text{O}$  with sodium benzoate and dmemH in a 2:4:1 ratio. Increasing the amount of sodium benzoate or dmemH still gave complex **1**, but the reaction was not so clean. Reactions in which MeCN was replaced by EtOH and  $\text{FeCl}_3 \cdot 6\text{H}_2\text{O}$  by  $\text{Fe}(\text{ClO}_4)_3 \cdot x\text{H}_2\text{O}$  or  $(\text{NEt}_4)_2(\text{Fe}_2\text{OCl}_6)$  also gave the same product for Fe/dmemH ratios of both 1:1 and 1:2. Clearly, complex **1** is a preferred product of these components and the particular carboxylate group.

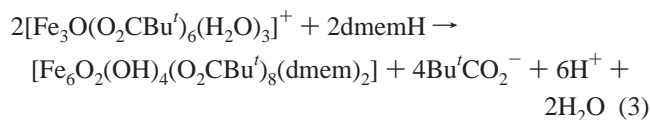
If the carboxylate employed was acetate instead of benzoate, then the product from the  $\text{FeCl}_3/\text{MeCO}_2\text{Na}/\text{dmemH}$  (2:5:1) reaction system in MeCN (method A of the Experimental Section) was another heptanuclear complex,  $[\text{Fe}_7\text{O}_4(\text{O}_2\text{CMe})_{11}(\text{dmem})_2]$  (**2**) (eq 2). Its formula is the same as that



of **1**, except for the carboxylate identity, but structurally the two complexes are very different (vide infra). The same product **2** was obtained using  $[\text{Fe}_3\text{O}(\text{O}_2\text{CMe})_6(\text{H}_2\text{O})_3](\text{NO}_3)$  as the starting material in a reaction with 2 equiv of dmemH in MeCN (method B). The yields of **2** were much lower than those of **1**, although they could be somewhat improved by the addition of some  $\text{NEt}_3$  base to the reaction.

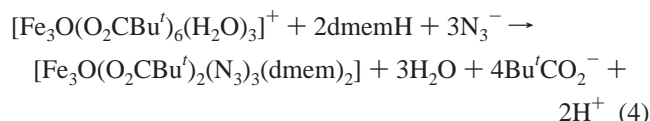
In contrast to the heptanuclear products from the use of benzoate and acetate reagents, the use of pivalate reagents

led to a hexanuclear product. Treatment of  $[\text{Fe}_3\text{O}(\text{O}_2\text{CBu}^t)_6(\text{H}_2\text{O})_3](\text{NO}_3)$  with dmemH in MeCN led to the subsequent isolation of  $[\text{Fe}_6\text{O}_2(\text{OH})_4(\text{O}_2\text{CBu}^t)_8(\text{dmem})_2]$  (**3**) (eq 3). The addition of 1 equiv of  $\text{NEt}_3$  or pyridine as a base improves the yield from 10 to 20%. The same product is obtained on increasing the amount of dmemH to 3 equiv.



It is clear that the reactions that lead to **1**–**3** are very complicated, and the reaction solutions likely contain a complicated mixture of several species in equilibrium. In such cases, factors such as relative solubility, lattice energies, crystallization kinetics, and others determine the identity of the isolated products, and one (or more) of these factors is undoubtedly the reason that the reaction product is so dependent on the exact carboxylate employed.

Since complex **3** contains bridging hydroxide groups, a similar reaction was explored in the presence of sodium azide. Perlepes and co-workers have demonstrated that the replacement of bridging hydroxide groups (which almost always mediate antiferromagnetic exchange interactions) with end-on bridging azide groups (which mediate ferromagnetic exchange) in cobalt, nickel, and iron clusters leads to products with much higher ground-state spin values.<sup>17</sup> Thus, we explored a variety of reaction conditions differing in the azide amount and/or solvent, and it was found that a reaction of  $[\text{Fe}_3\text{O}(\text{O}_2\text{CBu}^t)_6(\text{H}_2\text{O})_3](\text{NO}_3)$ , dmemH, and azide in a 1:2:4 ratio gave the new trinuclear complex  $[\text{Fe}_3\text{O}(\text{O}_2\text{CBu}^t)_2(\text{N}_3)_3(\text{dmem})_2]$  (**4**) (eq 4). The complex has its azide groups



all in terminal sites, but it nevertheless has an interesting core structure. Complex **4** was also obtained in lower yield from the reaction of preformed complex **3** with 4 equiv of sodium azide in EtOH.

**Description of Structures.** A labeled representation of complex **1** is shown in Figure 1. Selected interatomic distances and angles are summarized in Table 2. Complex **1**·4MeCN crystallizes in the monoclinic space group  $C2/c$  with the  $\text{Fe}_7$  molecule lying on a crystallographic  $C_2$  axis passing through the central Fe4 atom. The core can be described as two  $[\text{Fe}_4(\mu_3\text{O})_2]$  planar-butterfly units fused at body atom Fe4, with one butterfly unit being atoms Fe1', Fe2, Fe3, Fe4, O9, and O10'. Furthermore, each butterfly unit can be considered as two edge-sharing  $\text{Fe}_3\text{O}$  triangular units, with the  $\mu_3\text{-O}^{2-}$  bridging atoms O9 and O10 being

(16) (a) Takahashi, S.; Hill, S. *Rev. Sci. Instrum.* **2005**, *76*, 023114. (b) Mola, M.; Hill, S.; Goy P.; Gross, M. *Rev. Sci. Instrum.* **2000**, *71*, 186.

(17) (a) Boudalis, A. K.; Donnadieu, B.; Nastopoulos, V.; Clemente-Juan, J.; Modesto, M.; Alain, S.; Yiannis, T.; Jean-Pierre; Perlepes, S. P. *Angew. Chem., Int. Ed.* **2004**, *43*, 2266–2270. (b) Papaefstathiou, G. S.; Perlepes, S. P.; Escuer, A.; Vicente, R.; Font-Bardia, M.; Solans, X. *Angew. Chem., Int. Ed.* **2001**, *40*, 884–886. (c) Papaefstathiou, G. S.; Escuer, A.; Vicente, R.; Font-Bardia, M.; Solans, X.; Perlepes, S. P. *Chem. Commun.* **2001**, *23*, 2414–2415.

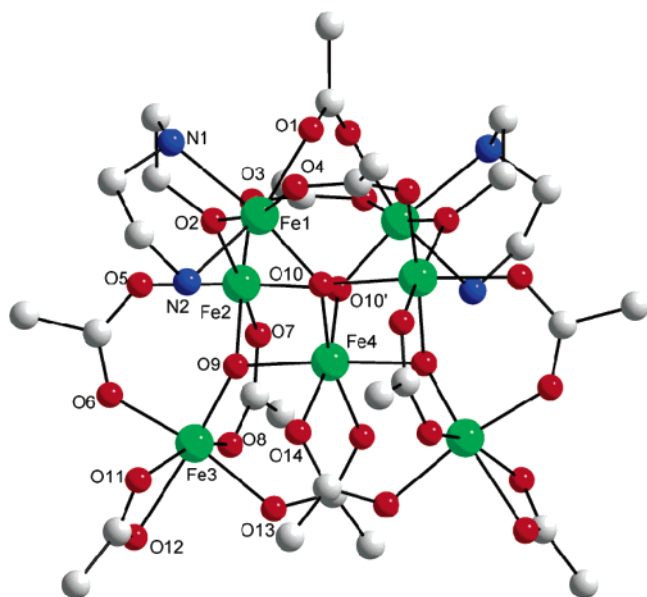


**Figure 1.** Labeled representation of the structure of **1**. Hydrogen atoms and phenyl rings (except for the ipso carbon atoms) have been omitted for clarity. The  $C_2$  symmetry axis is approximately vertical. Color code: Fe(III), green; O, red; N, blue; C, gray.

**Table 2.** Selected Bond Distances (Å) and Angles (deg) for **1**·4MeCN

Fe1–O10	1.8276(18)	Fe2–O7	2.1053(18)
Fe1–O2	1.9966(18)	Fe3–O9	1.8436(18)
Fe1–O4	2.0424(18)	Fe3–O8	2.0092(19)
Fe1–O1	2.0519(19)	Fe3–O6	2.027(2)
Fe1–N2	2.248(2)	Fe3–O13	2.038(2)
Fe1–N1	2.269(3)	Fe3–O11	2.0547(19)
Fe2–O9	1.9234(17)	Fe3–O12	2.200(2)
Fe2–O10	1.941(2)	Fe4–O9	1.989(2)
Fe2–O5	2.051(2)	Fe4–O10	1.9915(17)
Fe2–O2	2.0534(17)	Fe4–O14	2.0681(18)
Fe2–O3	2.0537(18)		
O10–Fe4–O10'	84.82(10)	Fe2–O9–Fe4	96.92(8)
Fe3–O9–Fe2	120.44(9)	Fe1–O10–Fe2	124.59(9)
Fe3–O9–Fe4	125.57(10)	Fe1–O10–Fe4	134.38(10)
Fe2–O10'–Fe4	96.25(8)		

slightly above and below their  $Fe_3$  planes. These O atoms bridge somewhat asymmetrically; the bonds to the wingtip Fe atoms ( $Fe1\cdots O10 = 1.828$  Å and  $Fe3\cdots O9 = 1.844$  Å) are shorter than the bonds to the body Fe atoms ( $Fe2\cdots O10' = 1.941$  Å and  $Fe2\cdots O9 = 1.923$  Å). The two  $dmem^-$  groups bind as tridentate chelates to Fe1 and its symmetry partner Fe1', with their alkoxide O atoms bridging wingtip atom Fe1 in one  $Fe_4$  unit with body atom Fe2 in the other. The remaining peripheral ligation about the  $[Fe_7O_4]$  core is provided by 11 benzoate groups, 9 in their common  $\eta^1:\eta^1:\mu$ -bridging mode and the other 2 in the rare  $\eta^2$ -chelating mode on Fe3 and Fe3'.

A labeled representation of complex **2** is provided in Figure 2. Selected interatomic distances and angles are given in Table 3. Complex **2**·MeCN crystallizes in the triclinic space group  $P\bar{1}$ . The molecule contains a remarkable  $[Fe_7(\mu_3-O)_4]$  core. It can be described as consisting of a central  $[Fe_3O_3]$  ring containing Fe2, Fe3, and Fe5, with each of the doubly bridging  $O^{2-}$  ions of this hexagon becoming  $\mu_3$  by also bridging to a third, external Fe atom (Fe1, Fe4, and Fe6). The fourth  $O^{2-}$  ion bridges ring atom Fe5, Fe6, and a

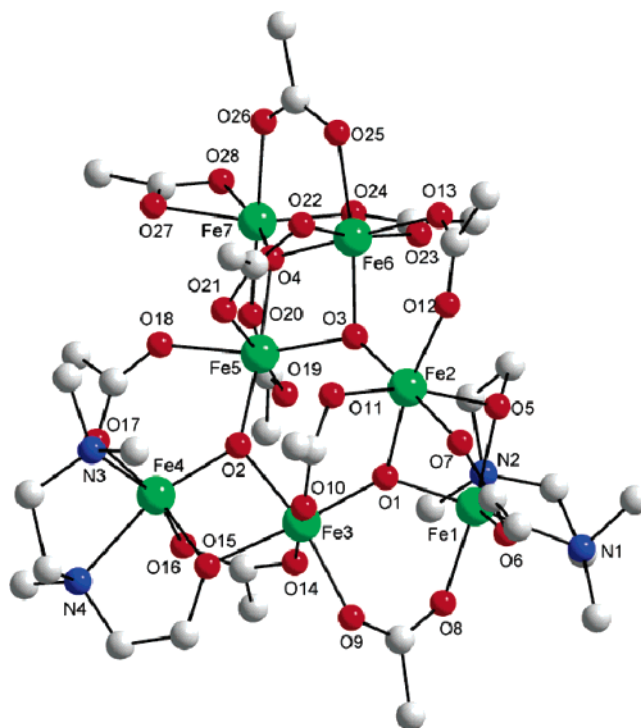


**Figure 2.** Labeled representation of the structure of **2**. Hydrogen atoms have been omitted for clarity. Color code: Fe(III), green; O, red; C, gray; N, blue.

**Table 3.** Selected Bond Distances (Å) and Angles (deg) for **2**·MeCN

Fe1–O1	1.8783(17)	Fe4–O17	2.0107(18)
Fe1–O6	1.9992(19)	Fe4–O15	2.057(2)
Fe1–O8	2.0106(18)	Fe4–N3	2.246(2)
Fe1–O5	2.0147(17)	Fe4–N4	2.268(2)
Fe1–N2	2.191(2)	Fe5–O2	1.9402(17)
Fe1–N1	2.282(2)	Fe5–O3	1.9568(17)
Fe2–O3	1.8672(17)	Fe5–O4	2.0141(17)
Fe2–O1	1.9833(18)	Fe5–O19	2.0554(19)
Fe2–O12	2.0291(18)	Fe5–O21	2.0590(19)
Fe2–O11	2.0413(19)	Fe5–O18	2.0922(18)
Fe2–O5	2.0541(18)	Fe6–O4	1.9053(18)
Fe2–O7	2.1647(18)	Fe6–O3	1.9579(17)
Fe3–O1	1.8621(17)	Fe6–O22	2.055(2)
Fe3–O2	1.9900(17)	Fe6–O25	2.0619(19)
Fe3–O16	2.0380(18)	Fe7–O4	1.8175(18)
Fe3–O10	2.0658(19)	Fe7–O24	2.011(2)
Fe3–O14	2.094(2)	Fe7–O27	2.0623(19)
Fe3–O9	2.0976(18)	Fe7–O26	2.069(2)
Fe4–O2	1.8787(17)	Fe7–O28	2.211(2)
Fe4–O16	1.9894(18)	Fe7–O20	2.057(2)
Fe6–O13	2.0416(18)		
Fe6–O23	2.0525(19)		
O3–Fe2–O1	93.57(7)	Fe2–O3–Fe5	128.04(9)
O1–Fe3–O2	98.58(7)	Fe2–O3–Fe6	129.56(9)
O2–Fe5–O3	104.52(7)	Fe5–O3–Fe6	95.88(7)
Fe3–O1–Fe1	133.53(10)	Fe7–O4–Fe6	121.04(9)
Fe3–O1–Fe2	123.22(9)	Fe7–O4–Fe5	132.30(10)
Fe1–O1–Fe2	99.98(8)	Fe6–O4–Fe5	95.69(7)
Fe4–O2–Fe5	127.18(9)	Fe1–O5–Fe2	93.29(7)
Fe4–O2–Fe3	99.52(8)	Fe4–O16–Fe3	94.35(7)
Fe5–O2–Fe3	130.01(9)		

seventh Fe atom (Fe7) on the periphery of the molecule. The two  $dmem^-$  groups bind one each to the external atoms Fe1 and Fe4 in a tridentate chelating manner, with their alkoxide O atoms also bridging to ring atoms Fe2 and Fe3, respectively. Peripheral ligation is completed by 11 acetate groups, 10 in  $\eta^1:\eta^1:\mu$ -bridging modes and 1  $\eta^2$  chelating to Fe7.

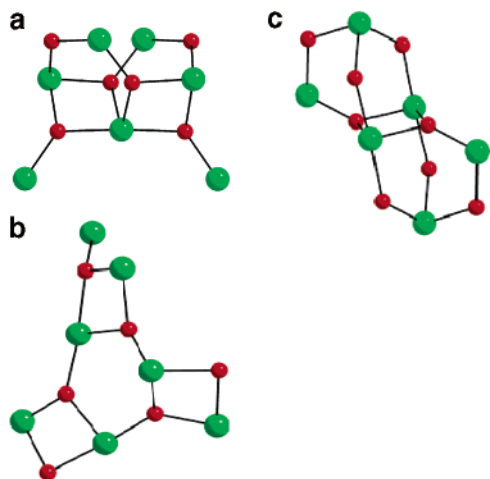


**Figure 3.** Comparison of cores of **1** (a), **2** (b), and **3** (c). Color code: Fe(III), green; O, red.

The molecular structures of **1** and **2** can be said to represent two different ways of linking a number of  $\text{Fe}_3\text{O}$  triangular units, as is clear in Figure 3, where the cores of **1–3** are compared. The core topologies of complexes **1** and **2** are unprecedented within Fe(III) chemistry. Indeed, there are only a few  $\text{Fe}_7$  complexes in the literature, and they are all mixed-valent except for the one reported by Winpenny and co-workers containing phenylphosphonate ligand and Zheng and co-workers containing cyclohexenephosphonate ligand.<sup>18</sup> While this manuscript was in preparation, disklike and domelike heptanuclear Fe(III) clusters were reported,<sup>19</sup> but they are structurally very different from complexes **1** and **2**; the latter are thus novel heptanuclear Fe(III) complexes.

A labeled representation of complex **3** is shown in Figure 4. Selected interatomic distances and angles are given in Table 4. Complex **3**·2MeCN crystallizes in the triclinic space group  $P\bar{1}$  with the asymmetric unit containing two independent  $\text{Fe}_6$  clusters, both lying on inversion centers; since the two molecules are essentially superimposable, we show and discuss the structure of only one of them here. The core consists of an  $[\text{Fe}_4(\mu_3\text{-O})_2]$  unit (Fe1, Fe1', Fe2, and Fe2'), on either side of which is attached a  $[\text{Fe}(\mu\text{-OH})_2(\mu\text{-OR})]$  unit containing Fe3; the  $\text{OH}^-$  ions are O9 and O10 on one side, and their symmetry partners are on the other side. One  $\text{OH}^-$  bridge (O10) connects Fe3 to central Fe1 whereas the other bridge (O9) connects to Fe2. The  $\text{OH}^-$  nature of O9 and O10 was confirmed by bond valence sum calculations,<sup>20</sup> which gave values of 1.14 for O9 and 1.05 for O10. Peripheral ligation is provided by two  $\text{dmem}^-$  and eight

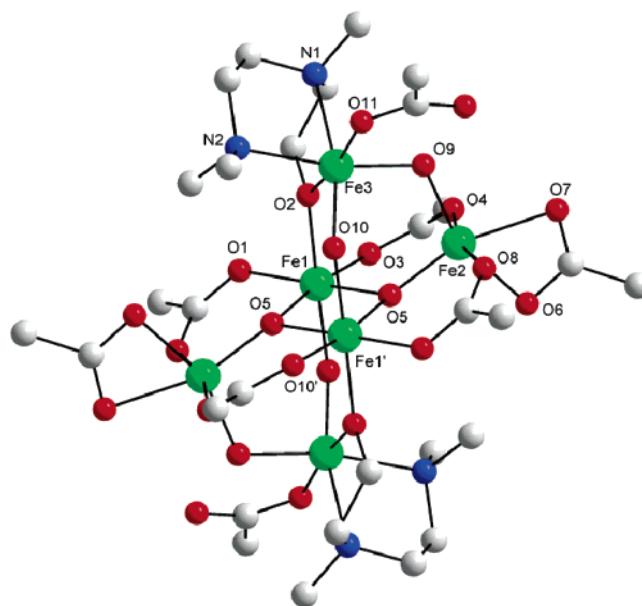


**Figure 4.** Labeled representation of the centrosymmetric structure of **3**. Hydrogen atoms and methyl groups on pivalate groups have been omitted for clarity. Color code: Fe(III), green; O, red; C, gray; N, blue.

**Table 4.** Selected Bond Distances (Å) and Angles (deg) for **3**·2MeCN

Fe1–O5	1.9382(17)	Fe2–O6	2.0662(19)
Fe1–O1	2.0251(18)	Fe2–O7	2.2189(19)
Fe1–O2	2.0457(17)	Fe3–O10	1.9420(17)
Fe1–O10'	2.0471(17)	Fe3–O9	1.9651(18)
Fe1–O3	2.0504(18)	Fe3–O2	2.0181(18)
Fe2–O5	1.8441(17)	Fe3–O11	2.0331(19)
Fe2–O9	1.9580(18)	Fe3–N1	2.231(2)
Fe2–O4	2.0412(18)	Fe3–N2	2.272(2)
Fe2–O8'	2.0448(18)		
Fe3–O2–Fe1	125.40(8)	Fe2–O9–Fe3	117.76(9)
Fe2–O5–Fe1	126.51(9)	Fe3–O10–Fe1'	129.75(9)
Fe1'–O5–Fe1	95.36(7)		

pivalate groups. There are three types of pivalate binding modes: four are in the common  $\eta^1\text{:}\eta^1\text{:}\mu$ -bridging mode, two are in the rare  $\eta^2$  chelating mode, and the remaining two are in an  $\eta^1$  terminal mode.

A number of other  $\text{Fe}_6$  complexes have been previously reported, possessing a variety of metal topologies, such as planar, twisted boat, chair, parallel triangles, octahedral, ladderlike, cyclic, etc.<sup>21</sup> However, the only previous compounds structurally similar to **3** are  $[\text{Fe}_6\text{O}_2(\text{OME})_{12}(\text{tren})_2]^{2-}$  (**5**)<sup>22</sup> and  $[\text{Fe}_6\text{O}_2(\text{OR})_8(\text{O}_2\text{CPh})_6]$  (**6**).<sup>23</sup> Both **5** and **6** contain

(18) (a) Tolis, E. I.; Helliwell, M.; Langley, S.; Raftery, J.; Winpenny, R. E. *Angew. Chem., Int. Ed.* **2003**, *42*, 3804–3808. (b) Yao, H.-C.; Li, Y.-Z.; Zheng, L.-M.; Xin, X.-Q. *Inorg. Chim. Acta* **2005**, *358*, 2523–2529.  
 (19) (a) Datta, S.; Betancur-Rodriguez, A.; Lee, S.-C.; Hill, S. O.; Foguet-Albiol, D.; Bagai, R.; Christou, G. *Polyhedron* **2007**, in press. DOI: 10.1016/j.poly.2006.11.006. (b) Jones, L. F.; Jensen, P.; Moubaraki, B.; Berry, K. J.; Boas, J. F.; Pilbrow, J. R.; Murray, K. R. *J. Mater. Chem.* **2006**, *16*, 2690–2697. (c) Ako, A. M.; Waldmann, O.; Mereacre, V.; Klöwer, F.; Hewitt, I. J.; Anson, C. E.; Güdel, H. U.; Powell, A. K. *Inorg. Chem. Acta* **2007**, *46*, 756–766.  
 (20) (a) Brown, I. D.; Altermatt, D. *Acta Crystallogr.* **1985**, *B41*, 244. (b) Palenik, G. J. *Inorg. Chem.* **1997**, *36*, 4888–4890. (c) Palenik, G. J. *Inorg. Chem.* **1997**, *36*, 122.

(21) (a) Seddon, E. J.; Huffman, J. C.; Christou, G. *Dalton* **2000**, *23*, 4446–4452. (b) Brechin, E. K.; Knapp, M. J.; Huffman, J. C.; Hendrickson, D. N.; Christou, G. *Inorg. Chim. Acta* **2000**, *297*, 389–399. (c) Cañada-Vilalta, C.; Rumberger, E.; Brechin, E. K.; Wernsdorfer, W.; Følting, K.; Davidson, E. R.; Hendrickson, D. N.; Christou, G. *J. Chem. Soc., Dalton Trans.* **2002**, *21*, 4005–4010. (d) Cañada-Vilalta, C.; O'Brien, T. A.; Pink, M.; Davidson, E. R.; Christou, G. *Inorg. Chem.* **2003**, *42*, 7819–7829. (e) Hegetschweiler, K.; Schmalke, H.; Streit, H. M.; Schneider, W. *Inorg. Chem.* **1990**, *29*, 3625–3627. (f) Christmas, C. A.; Tsai, H.; Lien, P.; Pardi, L.; Kesselman, J. M.; Gantzel, P. K.; Chadha, R. K.; Gatteschi, D.; Harvey, D. F.; Hendrickson, D. N. *J. Am. Chem. Soc.* **1993**, *115*, 12483–12490 and references therein. (g) Shweky, I.; Pence, L. E.; Papaefthymiou, G. C.; Sessoli, R.; Yun, J. W.; Bino, A.; Lippard, S. J. *J. Am. Chem. Soc.* **1997**, *119*, 1037–1042. (h) Grant, C. M.; Knapp, M. J.; Streib, W. E.; Huffman, J. C.; Hendrickson, D. N.; Christou, G. *Inorg. Chem.* **1998**, *37*, 6065–6070.  
 (22) Nair, V. S.; Hagen, K. S. *Inorg. Chem.* **1992**, *31*, 4048–4050.

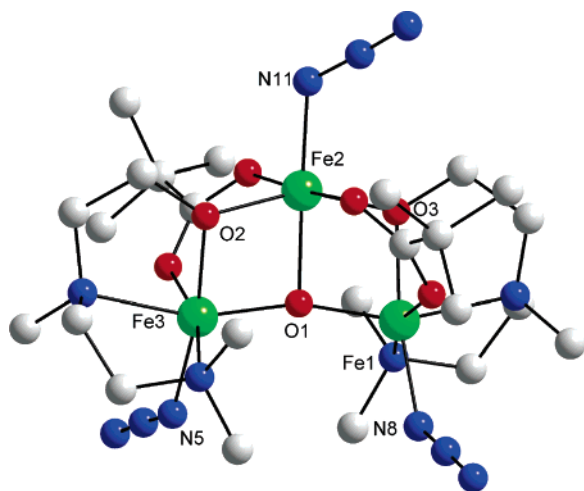


**Figure 5.** Labeled representation of the structure of **4**. Hydrogen atoms have been omitted for clarity. Color code: Fe(III), green; O, red; C, gray; N, blue.

**Table 5.** Selected Bond Distances (Å) and Angles (deg) for **4**·CH<sub>2</sub>Cl<sub>2</sub>

Fe1–O1	1.8716(19)	Fe2–O4	2.0469(19)
Fe1–N8	2.007(2)	Fe2–O6	2.0605(19)
Fe1–O3	2.0291(18)	Fe2–O1	2.0700(19)
Fe1–O7	2.0608(19)	Fe3–O1	1.8647(19)
Fe1–N4	2.220(2)	Fe3–N5	2.020(2)
Fe1–N3	2.243(2)	Fe3–O2	2.0245(19)
Fe2–O3	1.9787(19)	Fe3–O5	2.066(2)
Fe2–O2	1.9834(19)	Fe3–N2	2.211(2)
Fe2–N11	2.007(2)	Fe3–N1	2.241(2)
Fe3–O1–Fe1	162.82(11)	Fe2–O2–Fe3	96.07(8)
Fe3–O1–Fe2	98.34(8)	Fe2–O3–Fe1	96.77(8)
Fe1–O1–Fe2	98.85(8)		

a central [Fe<sub>4</sub>(μ<sub>3</sub>-O)<sub>2</sub>]<sup>8+</sup> core with an additional Fe atom on each side, as in **3**, but the precise means of attachment are different.

A labeled representation of **4** is provided in Figure 5. Selected interatomic distances and angles are given in Table 5. Complex **4**·CH<sub>2</sub>Cl<sub>2</sub> crystallizes in the monoclinic space group *P*2<sub>1</sub>/*n*. The structure consists of an Fe<sub>3</sub> isosceles triangle bridged by a μ<sub>3</sub>-O<sup>2-</sup> ion (O1) with a rare T-shaped geometry, rather than the common trigonal-planar geometry usually seen in triangular metal carboxylates.<sup>24</sup> The Fe1···Fe2 and Fe2···Fe3 edges are each additionally bridged by an alkoxide O atom of the dmem<sup>-</sup> ligand and a η<sup>1</sup>:η<sup>1</sup>:μ pivalate group. As a result, the Fe2···Fe1 (2.997(1) Å) and Fe2···Fe3 (2.980(1) Å) distances are much shorter than the Fe1···Fe3 (3.694(2) Å) distance. Similarly, the Fe2–O1 (2.070(19) Å) distance is noticeably longer than the Fe1–O1 (1.872(19) Å) and Fe3–O1 (1.865(19) Å) distances. Fe1, Fe2, Fe3, and O1 are coplanar, and O2 and O3 are slightly above and below this plane. A chelating dmem<sup>-</sup> and a terminal azide on each Fe atom complete the ligation at the metal atoms, which are all near-octahedral. The overall asymmetric Fe<sub>3</sub>O is with little precedent in iron chemistry,

(23) Ammala, P. S.; Batten, S. R.; Cashion, J. D.; Kepert, C. M.; Moubaraki, B.; Murray, K. S.; Spiccia, L.; West, B. O. *Inorg. Chim. Acta* **2002**, *331*, 90–97.

(24) Cotton, F. A.; Wilkinson, G. *Advanced Inorganic Chemistry*; Wiley: New York, 1980; pp 154–155.

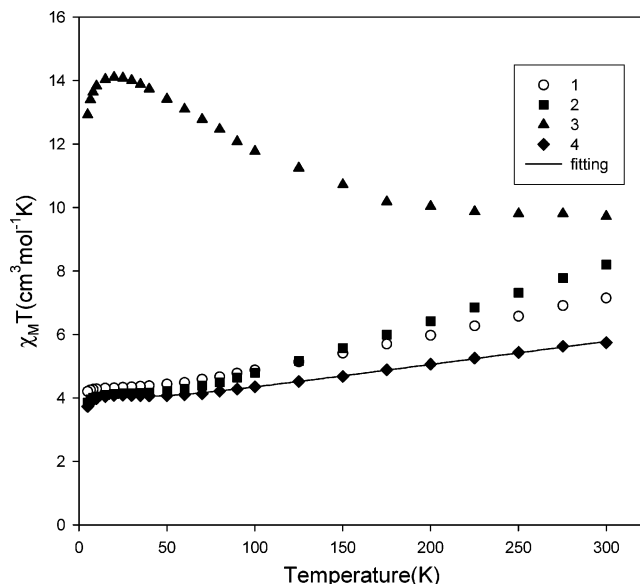


**Figure 6.** Plots of  $\chi_M T$  vs  $T$  for complexes **1** (○), **2** (■), **3** (▲), and **4** (◆). The solid line is the fit of the data for **4**; see the text for the fit parameters.

the only previous discrete example being [Fe<sub>3</sub>O(TIEO)<sub>2</sub>(O<sub>2</sub>-CPh)<sub>2</sub>Cl<sub>3</sub>], where TIEO is 1,1,2-tris(1-methylimidazol-2-yl)-ethoxide.<sup>25</sup>

**Magnetochemistry.** Solid-state, variable-temperature dc magnetic susceptibility data in a 0.1 T field and in the 5.0–300 K range were collected on powdered crystalline samples of **1–4** restrained in eicosane. The obtained data are plotted as  $\chi_M T$  vs  $T$  in Figure 6. For **1**· $\frac{1}{2}$ MeCN,  $\chi_M T$  steadily decreases from 6.95 cm<sup>3</sup> K mol<sup>-1</sup> at 300 K to 4.07 cm<sup>3</sup> K mol<sup>-1</sup> at 5.0 K. The 300 K value is much less than the spin-only ( $g = 2.0$ ) value of 30.62 cm<sup>3</sup> K mol<sup>-1</sup> for seven noninteracting Fe(III) ions, indicating the presence of strong antiferromagnetic interactions. The 5.0 K value suggests an  $S = \frac{5}{2}$  ground state. For **2**·2MeCN,  $\chi_M T$  steadily decreases from 8.19 cm<sup>3</sup> K mol<sup>-1</sup> at 300 K to 4.14 cm<sup>3</sup> K mol<sup>-1</sup> at 34 K, stays essentially constant until 10 K, and then decreases slightly to 3.85 cm<sup>3</sup> K mol<sup>-1</sup> at 5.0 K. As for **1**· $\frac{1}{2}$ MeCN, this behavior is indicative of antiferromagnetic interactions and an  $S = \frac{5}{2}$  ground state. For **3**,  $\chi_M T$  increases from 9.73 cm<sup>3</sup> K mol<sup>-1</sup> at 300 K to a maximum of 14.10 cm<sup>3</sup> K mol<sup>-1</sup> at 20 K and then drops to 12.92 cm<sup>3</sup> K mol<sup>-1</sup> at 5.0 K. The 300 K value is again much less than the spin-only value of 26.25 cm<sup>3</sup> K mol<sup>-1</sup> expected for six noninteracting Fe(III) ions, indicating predominantly antiferromagnetic interactions. The increase in  $\chi_M T$  as the temperature then decreases suggests that the lowest-lying states are of high-spin values, and the maximum at 20 K of 14.10 cm<sup>3</sup> K mol<sup>-1</sup> is very close to the spin-only value of 15.00 cm<sup>3</sup> K mol<sup>-1</sup> for an  $S = 5$  ground state. The decrease in  $\chi_M T$  at the lowest temperatures is very likely due to zero-field splitting (ZFS) within the  $S = 5$  ground state and perhaps some weak intermolecular interactions. For **4**· $\frac{1}{2}$ CH<sub>2</sub>Cl<sub>2</sub>,  $\chi_M T$  steadily decreases from 5.74 cm<sup>3</sup> K mol<sup>-1</sup> at 300 K to 4.07 cm<sup>3</sup> K mol<sup>-1</sup> at 50 K and then stays approximately constant until

(25) (a) Gorun, S. M.; Papaefthymiou, G. C.; Frankel, R. B.; Lippard, S. J. *J. Am. Chem. Soc.* **1987**, *109*, 4244–4255. (b) Gorun, S. M.; Lippard, S. J. *J. Am. Chem. Soc.* **1985**, *107*, 4568–4570.

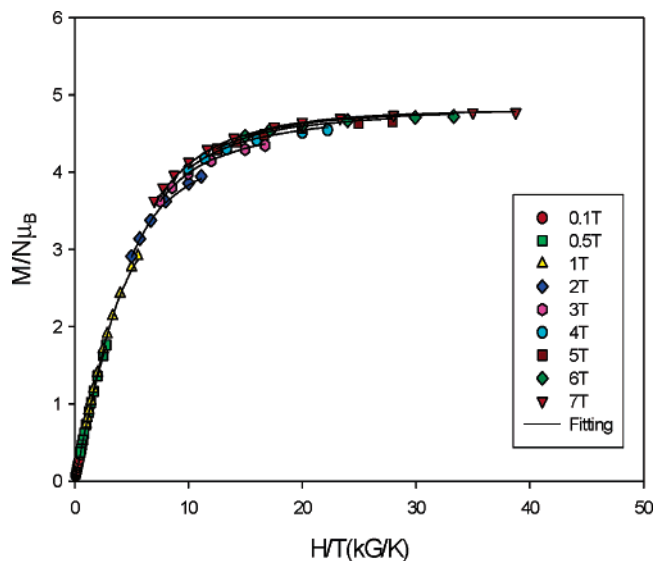


**Figure 7.** Plot of reduced magnetization ( $M/N\mu_B$ ) vs  $H/T$  for complex  $1 \cdot 1/2\text{MeCN}$ . The solid lines are the fit of the data; see the text for the fit parameters.

15 K, below which it decreases slightly to  $3.75 \text{ cm}^3 \text{ K mol}^{-1}$  at 5.0 K. The latter value suggests an  $S = 5/2$  ground state.

To confirm the above ground-state spin estimates, variable-field ( $H$ ) and temperature-magnetization ( $M$ ) data were collected in the 0.1–7.0 T and 1.8–10 K ranges. The resulting data for  $1 \cdot 1/2\text{MeCN}$  are plotted in Figure 7 as reduced magnetization ( $M/N\mu_B$ ) vs  $H/T$ , where  $N$  is Avogadro's number and  $\mu_B$  is the Bohr magneton. The saturation value at the highest fields and lowest temperatures is  $\sim 4.8$ , as expected for an  $S = 5/2$  spin state and with  $g$  slightly less than 2; the saturation value should be  $gS$ . The data were fit, using the program *MAGNET*,<sup>26</sup> by diagonalization of the spin Hamiltonian matrix assuming that only the ground state is populated, incorporating axial anisotropy ( $D\hat{S}_z^2$ ) and Zeeman terms, and employing a full powder average. The corresponding spin Hamiltonian is given by eq 5, where  $\hat{S}_z$  is the easy-axis spin operator,  $g$  is the Landé  $g$  factor,  $\mu_0$  is the vacuum permeability, and  $H$  is the applied

$$H = D\hat{S}_z^2 + g\mu_B\mu_0\hat{S}\cdot H \quad (5)$$

field. The last term in eq 5 is the Zeeman energy associated with an applied magnetic field. The best fit for  $1 \cdot 1/2\text{MeCN}$  is shown as the solid lines in Figure 7 and was obtained with  $S = 5/2$  and with either of two sets of parameters,  $g = 1.94$  and  $D = -0.56 \text{ cm}^{-1}$  or  $g = 1.95$  and  $D = 0.77 \text{ cm}^{-1}$ . Alternative fits with  $S = 3/2$  or  $7/2$  were rejected because they gave unreasonable values of  $g$  and  $D$ . It should be noted that it is common to obtain two acceptable fits of magnetization data for a given  $S$  value, one with  $D > 0$  and the other with  $D < 0$ . This was indeed the case for the magnetization fits for all of the complexes **1–4** in this work. To assess which is the superior fit in these cases and to also ensure that the true global minimum had been located for each compound, we calculated the root-mean-square error surface

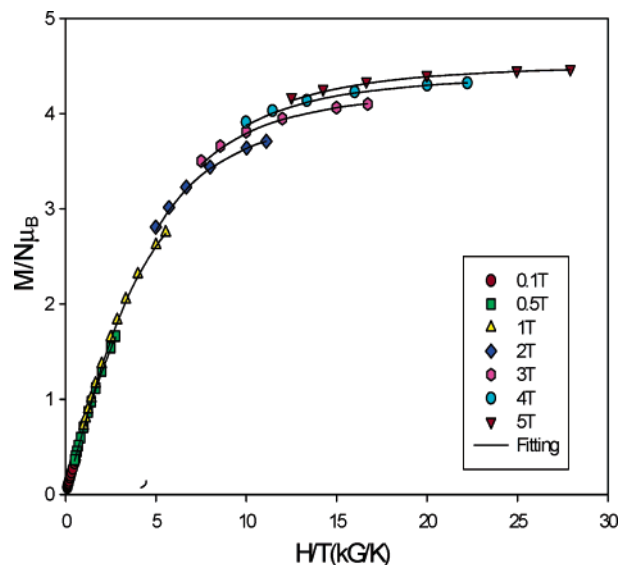


**Figure 8.** Plot of reduced magnetization ( $M/N\mu_B$ ) vs  $H/T$  for  $2 \cdot 2\text{MeCN}$ . The solid lines are the fit of the data; see the text for the fit parameters.

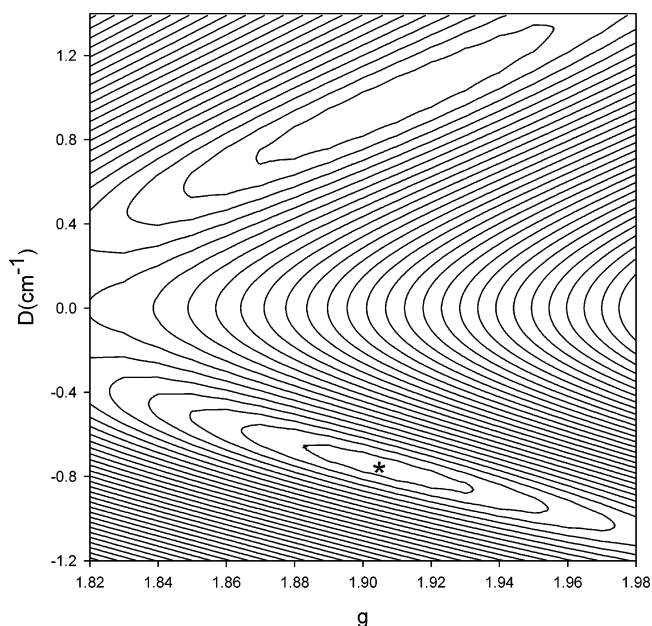


**Figure 9.** Two-dimensional contour plot of the fitting-error surface vs  $D$  and  $g$  for  $2 \cdot 2\text{MeCN}$ .

for the fits as a function of  $D$  and  $g$  and have plotted them as two-dimensional contour plots. We will show below the data for  $2 \cdot 2\text{MeCN}$  as the representative example; the rest are available as Supporting Information. For  $1 \cdot 1/2\text{MeCN}$  (Supporting Information, Figure S1), the plot clearly shows only the above-mentioned minima with positive and negative  $D$  values, with both fits being of comparable quality.

For  $2 \cdot 2\text{MeCN}$ , the reduced magnetization plot saturates at  $\sim 4.5$ , again suggesting an  $S = 5/2$  ground state (Figure 8). The fit, shown as the solid lines in Figure 8, gave  $S = 5/2$  with either  $g = 1.91$  and  $D = -0.76 \text{ cm}^{-1}$  or  $g = 1.91$  and  $D = 0.98 \text{ cm}^{-1}$ . The error surface contour plot is shown in Figure 9 and shows the above minima, with the one with negative  $D$  clearly the superior fit since it has a lower (deeper) minimum. Figure 9 also clearly shows that the fit

(26) Davidson, E. R. *MAGNET*; Indiana University: Bloomington, IN, 1999.

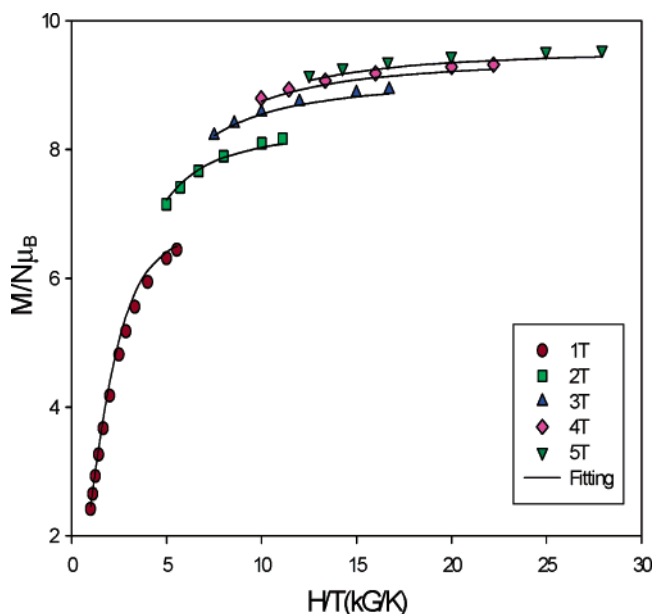
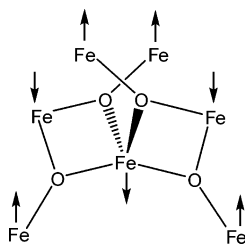


**Figure 10.** Plot of reduced magnetization ( $M/N\mu_B$ ) vs  $H/T$  for complex **3**. The solid lines are the fit of the data; see the text for the fit parameters.

#### Scheme 1



minimum is a soft one, consistent with significant uncertainty in the precision of the obtained  $g$  and  $D$  fit values, which we estimate as  $\pm 0.02$  on  $g$  and  $\pm 5$ – $10\%$  on  $D$ .

For **3**, the reduced magnetization plot saturates at  $\sim 9.5$ , suggesting an  $S = 5$  state with  $g < 2$  (Figure 10). A satisfactory fit could only be obtained if data collected at fields above 5 T were excluded, suggesting that some low-lying excited states with  $S > 5$  are being stabilized by the applied field to the point that they are significantly populated at these temperatures. To avoid this, the data at 6 and 7 T were excluded, and now a good fit was obtained (solid lines in Figure 10) with  $S = 5$  and either  $g = 1.95$  and  $D = -0.28 \text{ cm}^{-1}$  or  $g = 1.92$  and  $D = 0.33 \text{ cm}^{-1}$ . The error surface for the fit shows again that the fit with negative  $D$  is far superior (Supporting Information, Figure S2), suggesting that this is the true sign of  $D$ .

It is of interest to try to rationalize the observed ground-state spin values of **1**–**3**. It is assumed that all  $\text{Fe}_2$  pairwise exchange interactions are antiferromagnetic, as is essentially always the case for high-spin  $\text{Fe(III)}$ , and there will thus be competing antiferromagnetic exchange interactions and spin-frustration effects within the many  $\text{Fe}_3$  triangular units in these complexes. The ground state of **1** is the easiest to rationalize: the discrete  $\text{Fe}_4$  butterfly (planar or bent rhombus) topology is known to usually give an  $S = 0$  ground state as a result of the antiferromagnetic interactions along the four outer edges, overcoming, and thus frustrating, the

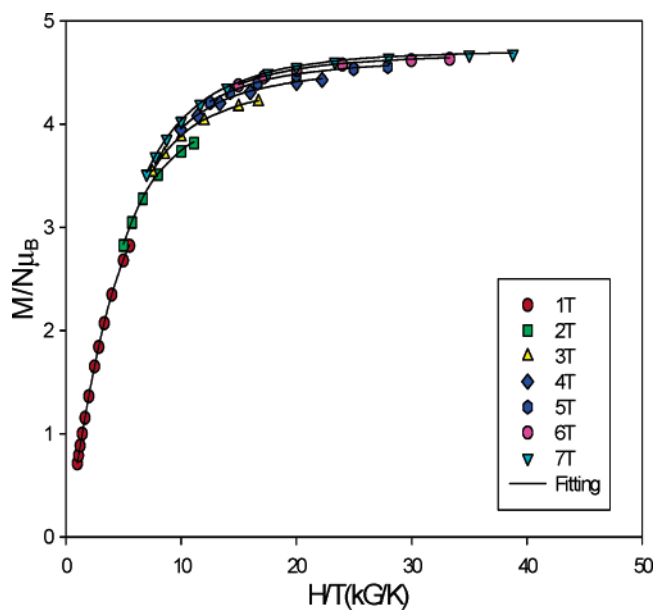


**Figure 11.** Plot of reduced magnetization ( $M/N\mu_B$ ) vs  $H/T$  for complex **4**. The solid lines are the fit of the data; see the text for the fit parameters.

diagonal interaction.<sup>7,27</sup> In **1**, two such  $\text{Fe}_4$  units are fused at the body (central)  $\text{Fe}_4$  of the two butterfly units and, assuming the same spin alignments as those in the discrete  $\text{Fe}_4$  molecules, the ground-state spin alignments are predicted to be those shown in Scheme 1, giving an  $S = 5/2$  ground state, as observed experimentally. The structurally different  $\text{Fe(III)}_7$  complexes mentioned above with disklike and domelike topologies also possess  $S = 5/2$  ground states.<sup>19</sup>

The ground states for **2** and **3** are not so easy to rationalize convincingly because of their high content of triangular units, especially for **2**. For **3**, the recognizable  $\text{Fe}_4$  unit as in **1** suggests that the spin of this subunit is zero, and then the two Fe atoms  $\text{Fe}_3$  and  $\text{Fe}_3'$  above and below would have their spins parallel to each other by both being antiparallel to the spins of  $\text{Fe}_1$  and  $\text{Fe}_1'$ . This would thus rationalize an overall  $S = 5$  ground state for **3**.

For  $4 \cdot 1/2 \text{CH}_2\text{Cl}_2$ , the reduced magnetization saturates at  $\sim 4.7$ , suggesting an  $S = 5/2$  ground state and  $g < 2$  (Figure 11). The fit of the data (solid lines in Figure 11) gave  $S = 5/2$  with either  $g = 1.92$  and  $D = -0.69 \text{ cm}^{-1}$  or  $g = 1.92$  and  $D = 0.82 \text{ cm}^{-1}$ . The  $D$  vs  $g$  error surface (Supporting Information, Figure S3) shows that the fit with negative  $D$  is again superior, suggesting that this may be the true sign of  $D$ . Since complex **4** is only trinuclear, we determined its pairwise  $\text{Fe}_2$  exchange interactions by fitting the variable-temperature susceptibility data to the appropriate theoretical expression.

- (27) (a) Wemple, M. W.; Coggin, D. K.; Vincent, J. B.; McCusker, J. K.; Strieb, W. E.; Huffman, J. C.; Hendrickson, D. N.; Christou, G. *J. Chem. Soc., Dalton Trans.* **1998**, 4, 719–725. (b) Boudalis, A. K.; Tangoulis, V.; Raptopoulou, C. P.; Terzis, A.; Tchuagues, J.-P.; Perlepes, S. P. *Inorg. Chim. Acta* **2004**, 357, 1345–1354. (c) Overgaard, J.; Hibbs, D. E.; Rentschler, E.; Timco, G. A.; Larsen, F. K. *Inorg. Chem.* **2003**, 42, 7593–7601. (d) Boudalis, A. K.; Lalioti, N.; Spyroulias, G. A.; Raptopoulou, C. P.; Terzis, A.; Bousseksou, A.; Tangoulis, V.; Tchuagues, J.-P.; Perlepes, S. P. *Inorg. Chem.* **2002**, 41, 6474–6487. (e) Chaudhuri, P.; Rentschler, E.; Birkelbach, F.; Krebs, C.; Bill, E.; Weyhermüller, T.; Flörke, U. *Eur. J. Inorg. Chem.* **2003**, 541–555.

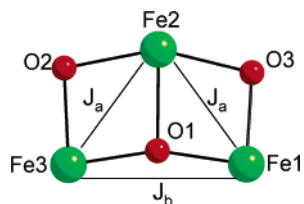
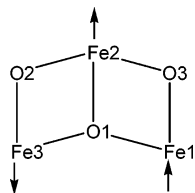


Figure 12. Core of **4** defining the pairwise exchange interactions.

#### Scheme 2



The Heisenberg spin Hamiltonian describing the isotropic exchange interactions within an isosceles Fe<sub>3</sub> triangle of *C*<sub>2v</sub> symmetry (Figure 12) is given by eq 6, where *J*<sub>a</sub> refers to the interactions between Fe2•••Fe3 and Fe1•••Fe2 and *J*<sub>b</sub> refers to the Fe3•••Fe1 interaction; *S*<sub>*i*</sub> refers to the spin of atom Fe<sub>*i*</sub>.

$$H = -2J_a(\hat{S}_2 \cdot \hat{S}_3 + \hat{S}_2 \cdot \hat{S}_1) - 2J_b(\hat{S}_3 \cdot \hat{S}_1) \quad (6)$$

The energies of the resultant total spin states *S*<sub>T</sub>, which are eigenfunctions of the Hamiltonian in this coupling scheme, are given by eq 7, where  $\hat{S}_A = \hat{S}_1 + \hat{S}_3$ . The overall multiplicity of the spin system is 216, made up of 27 individual spin states ranging from *S*<sub>T</sub> = 1/2 to 15/2.

$$E|S_T, S_A\rangle = -J_a[S_T(S_T + 1) - S_A(S_A + 1)] - J_b[S_A(S_A + 1)] \quad (7)$$

An expression for the molar paramagnetic susceptibility was derived for this complex using the Van Vleck equation.<sup>28</sup> This was then used to fit the experimental  $\chi_M T$  vs *T* data, with fit parameters of *J*<sub>a</sub>, *J*<sub>b</sub>, and an isotropic *g* value. The fit is shown as the solid line in Figure 6, which gave *J*<sub>a</sub> = -3.6 cm<sup>-1</sup>, *J*<sub>b</sub> = -45.9 cm<sup>-1</sup>, and *g* = 1.93. These values identify the ground state as the |*S*<sub>T</sub>, *S*<sub>A</sub>⟩ = |5/2, 0⟩ state shown in Scheme 2, which is in agreement with the conclusion from the reduced magnetization fit. Clearly, the antiferromagnetic *J*<sub>a</sub> interaction is totally frustrated by the much stronger *J*<sub>b</sub> interaction, and the spins of Fe1 and Fe3 are thus aligned antiparallel.

The marked inequality in the exchange constants, |*J*<sub>b</sub>| ≫ |*J*<sub>a</sub>|, is as expected on the basis of the iron–oxo bond lengths, where Fe3–O1 = Fe1–O1 < Fe2–O1. A similar situation was also observed in the previous Fe<sub>3</sub> complex with a similar core, [Fe<sub>3</sub>O(TIEO)<sub>2</sub>(O<sub>2</sub>CPh)<sub>2</sub>Cl<sub>3</sub>], for which *J*<sub>a</sub> = -8(4) cm<sup>-1</sup> and *J*<sub>b</sub> = -55(6) cm<sup>-1</sup>. It has been established that the magnitude of the exchange coupling constant *J* for an oxo-bridged Fe(III)<sub>2</sub> unit can be approximately correlated with a single structural parameter *P* by the expression in eq 8 if

the Fe–O–Fe angle does not alter too much. In this

$$-J = Ae^{BP} \quad (8)$$

relationship, *A* = 8.763 × 10<sup>11</sup>, *B* = -12.663, and *P* is the shortest superexchange pathway.<sup>29</sup> Applying this relationship to complex **4** gives *J*<sub>a</sub> = -12.9 cm<sup>-1</sup> and *J*<sub>b</sub> = -46.4 cm<sup>-1</sup>, which are in reasonable overall agreement with the experimental values obtained from fitting the susceptibility data, especially since it is assumed reasonable that an angular dependence is of lesser importance than the radial one, and this is ignored by eq 8. However, the acute values of the angles of Fe2–O2–Fe3 and Fe2–O3–Fe1 (96.07(8) and 96.77(8) Å, respectively), which lead to the weak *J*<sub>a</sub> coupling, are significantly smaller than those found in dinuclear Fe(III)<sub>2</sub> complexes on which the relationship of eq 8 was based and probably do reflect an angular dependence. The value of *J*<sub>b</sub> is stronger than the magnitude of the antiferromagnetic coupling constant found for the triangular iron(III) carboxylate complexes with an approximately equilateral [Fe<sub>3</sub>O]<sup>7+</sup> core (~30 cm<sup>-1</sup>)<sup>30</sup> but weaker than the 80–130 cm<sup>-1</sup> values observed for the [Fe<sub>2</sub>O]<sup>4+</sup> and [Fe<sub>2</sub>O(O<sub>2</sub>CR)<sub>2</sub>]<sup>2+</sup> dinuclear cores.<sup>31</sup>

None of the compounds **1–4** exhibited an out-of-phase ac magnetic susceptibility signal down to 1.8 K in an ac field of 3.5 Oe oscillating with frequencies up to 997 Hz. This indicates that they do not exhibit a large enough barrier (vs *kT*) to exhibit the characteristic signature of slow magnetization relaxation characteristic of SMMs, at least down to 1.8 K.

As discussed above, fits of variable-temperature and variable-field magnetization data are not the most reliable way to obtain the most precise and accurate values of *D* or its sign. The magnetization fits suggested *D* to be negative for **2** and **3**, but they could not suggest the sign of *D* for **1**. Since the sign and magnitude of *D* are crucial to the potential ability of a complex to function as a SMM, we desired to better characterize *D* for these new and relatively rare examples of Fe<sub>x</sub> clusters with significant ground-state spin values. The perfect technique for this is HFEPR spectroscopy.

**HFEPR Spectroscopy.** A detailed single-crystal study of representative complexes **1**·4MeCN and **3**·2MeCN has been carried out by HFEPR spectroscopy. The main overall objective was to measure the ZFS parameters in the spin Hamiltonian of eq 9

$$H = D\hat{S}_z^2 + E(\hat{S}_x^2 - \hat{S}_y^2) + g\mu_B\mu_0\hat{S}\cdot H \quad (9)$$

which is the same as that in eq 5 except that it also now includes the rhombic ZFS term, *E*( $\hat{S}_x^2 - \hat{S}_y^2$ ), where *E* is the rhombic ZFS parameter and  $\hat{S}_x$  and  $\hat{S}_y$  are the *x* and *y*

(29) Gorun, S. M.; Lippard, S. J. *Inorg. Chem.* **1991**, *30*, 1625–1630.

(30) Dziobkowski, C. T.; Wroblewski, J. T.; Brown, D. B. *Inorg. Chem.* **1981**, *20*, 671–678.

(31) (a) Armstrong, W. H.; Lippard, S. J. *J. Am. Chem. Soc.* **1983**, *105*, 4837–4838. (b) Armstrong, W. H.; Spool, A.; Papaefthymiou, G. C.; Frankel, R. B.; Lippard, S. J. *J. Am. Chem. Soc.* **1984**, *106*, 3653–3667. (c) Armstrong, W. H.; Lippard, S. J. *J. Am. Chem. Soc.* **1985**, *107*, 3730–3731.

(28) Van Vleck, J. H. *The Theory of Electric and Magnetic Susceptibilities*; Oxford Press: London, 1932.

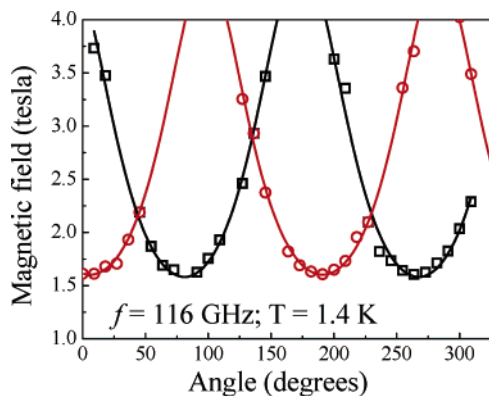


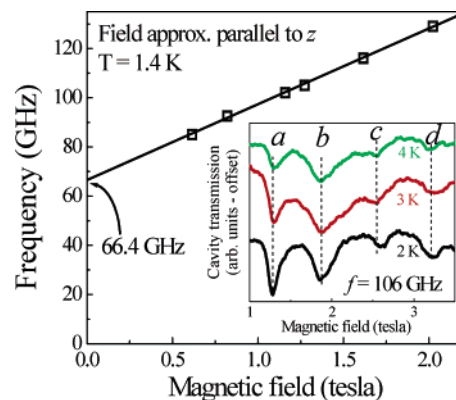
**Figure 13.** Plot of the HF EPR peak positions for  $3\cdot 2\text{MeCN}$  obtained from angle-dependent studies at 116 GHz and 1.4 K.

components of the total spin operator  $\hat{S}$ . EPR is a high-resolution spectroscopic technique that can be used to investigate the more complete spin Hamiltonian of eq 9, whereas fits of bulk magnetization data are essentially insensitive to inclusion of the rhombic  $E$  term.

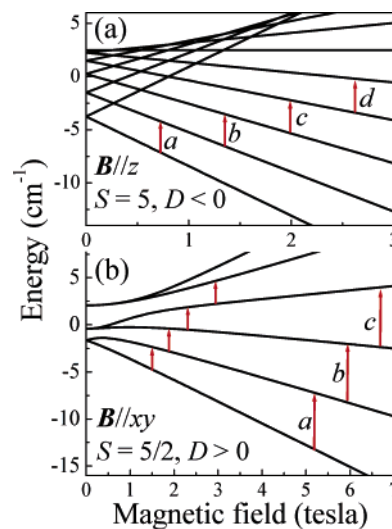
Single-axis angle-dependence studies were first performed to roughly determine the orientation of each crystal in the magnetic field. Both complexes  $1\cdot 4\text{MeCN}$  and  $3\cdot 2\text{MeCN}$  possess low-symmetry structures. Thus, determining the precise symmetry directions represents a highly complex task requiring detailed two-axis rotation studies. However, as we have recently demonstrated for several other low-symmetry polynuclear complexes, one can readily obtain basic information from single-axis studies,<sup>19a,32</sup> in particular, the sign of  $D$ , which is the crucial factor in whether a particular complex is a SMM.

Figure 13 displays the angle dependence of the field positions of the strongest EPR transitions determined from field-swept spectra recorded at 116 GHz and 1.4 K for complex  $3\cdot 2\text{MeCN}$ ; given the low temperature, these data points must correspond to transitions from the lowest-lying  $m_S$  levels. Two series of resonances are observed (black and red data points), which shift significantly upon rotation of the field, thus providing the clearest evidence for a significant magnetoanisotropy. Both series exhibit  $180^\circ$  periodicity, with virtually identical amplitudes. The source of the two series has a natural explanation for complex  $3\cdot 2\text{MeCN}$  for which there are two differently oriented molecules in the unit cell. Thus, one naturally expects two distinct EPR signatures, one from each orientation. The solid curves represent phenomenological fits to the two sets of data and are intended to capture the qualitative nature of the angle dependence. The phase shift between the two data sets is  $75 \pm 2^\circ$ .

To determine the sign of  $D$ , frequency- and temperature-dependent data were collected on complex  $3\cdot 2\text{MeCN}$  with the field oriented along one of the minima in Figure 13 (191°). Figure 14 displays the frequency dependence of the angle-dependent peak from Figure 13, and the inset displays representative spectra taken at higher temperatures. A remarkable feature of the frequency-dependent data is that



**Figure 14.** Frequency dependence for  $3\cdot 2\text{MeCN}$  with the field oriented along one of the minima in Figure 13 (191°). The inset displays temperature-dependent spectra obtained at 106 GHz.



**Figure 15.** (a) Simulated Zeeman diagram for a spin  $S = 5$  system with  $D < 0$ , with the magnetic field parallel to the  $z$  axis. The red lines (labeled a–d) correspond to the transitions shown in the inset of Figure 14. (b) Simulated Zeeman diagram for a spin  $S = 5/2$  system with  $D > 0$ , with the magnetic field parallel to the  $xy$  plane. The red lines (labeled a–c) correspond to the transitions shown in Figure 16.

all peaks lie on a straight line, which extrapolates to a finite frequency on the vertical axis; i.e., there is no evidence for curvature in the data. Assuming  $|DS| \approx 1.5 \text{ cm}^{-1}$  (from reduced magnetization measurements), one realizes that at least a 3 T magnetic field would be required to overcome the axial term in eq 9. This suggests that the Zeeman interaction commutes with the dominant axial term in eq 9 across the entire range of fields for which data were collected (0.6–2 T). In other words, the minima in Figure 13 and the data in Figure 14 correspond to field orientations parallel to or very close to the  $z$  axes of the two species. This is quite coincidental, as the sample orientation was not previously known.

Figure 15a displays a simulation of the Zeeman diagram for a SMM with  $S = 5$ , i.e., with  $D < 0$ . As can clearly be seen, the transition from the lowest-lying  $m_S$  level occurs at the lowest field; the excited-state transitions all occur at higher field. This agrees qualitatively with the data in Figure 14. Therefore, we can conclude that  $D$  is negative and that  $3$  is a SMM. The intercept on the frequency axis in Figure

(32) Lee, S.-C.; Stamatatos, T. C.; Hill, S.; Perlepes, S. P.; Christou, G. *Polyhedron*, in press. DOI:10.1016/j.poly.2006.10.052.

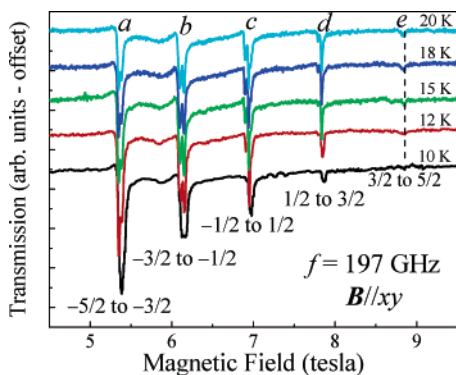


**Figure 16.** Temperature-dependent spectra for **1·4MeCN** at 197 GHz with the dc magnetic field applied within the easy ( $xy$ ) plane.

14 (66.4 GHz) then corresponds to the ZFS between the ground and first excited states. If one assumes that  $S = 5$ , then  $D = -0.25(1) \text{ cm}^{-1}$ , which is in reasonable agreement with the value from the magnetization fits ( $D = -0.28(3) \text{ cm}^{-1}$ ). Because of the uncertainty in the precise orientation of the field relative to the easy axis, we cannot quote a precise value for  $g$ ; the main purpose of the HFEPR measurements was to unambiguously determine the sign of  $D$ , which was successfully achieved.

Single-axis rotation experiments for complex **1·4MeCN** were not able to locate the axial direction (presumably, the rotation plane was inclined significantly with respect to the magnetic  $z$  axis of the molecule). Nevertheless, we were able to locate the plane perpendicular to the axial direction ( $xy$  plane) from measurements similar to those shown in Figure 13. Thus, all of the temperature- and frequency-dependent studies were carried out with the field aligned within the magnetic  $xy$  plane of the  $\text{Fe}_7$  molecule. Only a single molecular species was anticipated for complex **1·4MeCN**, making interpretation of the data more straightforward. Furthermore, this complex exhibits sharper EPR peaks, as evident from Figure 16, which shows the high-field  $xy$ -plane spectra obtained at different temperatures and a frequency of 197 GHz. Comparison of the data in Figure 16 with the simulated Zeeman diagram in Figure 15b reveals that complex **1 cannot be** a SMM because its  $D$  value is positive. As can be seen from Figure 15b, upon reduction of the temperature, the stronger EPR peaks should be observed at the lowest fields for an easy-plane magnet ( $D > 0$ ) when the field is applied parallel to the easy ( $xy$ ) plane; this is exactly what is seen in the data. If **1·4MeCN** were a SMM, the intensities of the five transitions (labeled a–e in Figure 16) would be reversed.

Figure 17 displays the results of a multifrequency study for complex **1·4MeCN**, with the field applied within the easy plane; the temperature was 20 K. Fits (solid curves) to the positions of the EPR peaks were performed via exact diagonalization of eq 9. It is very clear from Figure 17 that the data lie on a series of lines that are *not* evenly spaced and exhibit significant curvature at low frequencies and fields. These trends are a characteristic of  $xy$ -plane spectra obtained for a system with a significant uniaxial anisotropy (both positive and negative  $D$ ), due to the competition

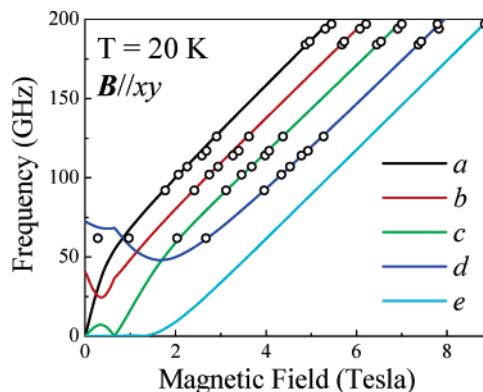


**Figure 17.** Easy-plane peak positions for **1·4MeCN** plotted vs frequency at 20 K. The solid lines are simulations made using the ZFS parameters given in the main text.

between the orthogonal Zeeman and ZFS ( $DS_z^2$ ) interactions. In other words, the data displayed in Figure 17 provide further confirmation that the field is in the  $xy$  plane and, when combined with the temperature dependence in Figure 16, also confirm the positive sign of  $D$ . The fit assumes an  $S = 5/2$  ground state and yields values of  $g = 2.0$  and  $D = +0.62 \text{ cm}^{-1}$ . This value again agrees reasonably well with that from the reduced magnetization studies ( $D = +0.77(7) \text{ cm}^{-1}$ ). The somewhat lower value of  $g$  obtained from the reduced magnetization fits is due to the lower precision available from bulk magnetization fits and also to the assumption of axial anisotropy in the latter; HFEPR data are more reliable. In fact, the best fit to the HFEPR data required the inclusion of a rhombic ZFS anisotropy,  $|E| \geq 0.067 \text{ cm}^{-1}$ . This is not unexpected, given the low symmetry of the molecule. Our estimate of  $E$  represents a lower bound, as the orientation of the field within the easy plane was not known. Low-temperature EPR measurements on the dome-like  $\text{Fe(III)}_7$  cluster yield a  $D$  value of  $0.28 \text{ cm}^{-1}$ ,<sup>19b</sup> which is considerably lower than that for **1·4MeCN**. This can be attributed to their different structural arrangements leading to the differences in single-ion anisotropy and spin–spin anisotropy.

## Conclusions

The tridentate N,N,O ligand  $\text{dmem}^-$  has proven to be a very fruitful new route to a variety of new  $\text{Fe(III)}$  clusters comprising two  $\text{Fe}_7$  and one  $\text{Fe}_6$  species, depending on the identity of the carboxylate employed. The latter point emphasizes the exquisite sensitivity of the reaction product on a variety of reaction conditions and reagents employed. For example, even though complexes **1** and **2** have the same formula except for the identity of the carboxylate, the structures of the two complexes are very different. It was interesting that the azide ligands in **4** were only terminal rather than bridging but, nevertheless, fostered formation of a product very different from that of the non-azide product **3**.

Fitting of the reduced magnetization vs  $H/T$  data established that **1**, **2**, and **4** each possesses an  $S = 5/2$  ground state spin, whereas **3** has an  $S = 5$  ground state. The complexes all serve to clearly emphasize again how ground-state spin

values of significant magnitude can result from spin-frustration effects even though all the pairwise exchange-interaction constants are antiferromagnetic. The magnetization fits of **1–4** serve to emphasize, however, the difficulty of determining the sign of  $D$  for Fe(III) clusters from such measurements, thus making it difficult to predict whether a given cluster might be a new example of a SMM. Representative complexes **1** and **3** were therefore studied by HFEPR spectroscopy, a tremendously powerful and sensitive technique, useful for obtaining accurate and precise values for spin Hamiltonian parameters such as  $D$ , including an unequivocal determination of its sign. From these measurements, we concluded that complex **3** has  $D < 0$  and thus is a potential SMM, whereas complex **1** has  $D > 0$  and is not a potential SMM. In fact, none of the compounds **1–4** exhibited an out-of-phase ac magnetic susceptibility signal down to 1.8 K in ac frequencies up to 997 Hz. Even for **3**, which was confirmed by HFEPR spectroscopy to have a negative  $D$  value, its values of  $S = 5$  and  $D = -0.25 \text{ cm}^{-1}$  give a barrier ( $U$ ) to magnetization relaxation with an upper value of  $U = S^2|D| = 6.3 \text{ cm}^{-1}$  ( $=9.0 \text{ K}$ ). Remembering that the true or effective barrier ( $U_{\text{eff}}$ ) is less than  $U$  due to

quantum tunneling of the magnetization through the barrier,<sup>3</sup> it is not surprising that no sign of slow relaxation is seen at temperatures above 1.8 K. Studies done at temperatures significantly below 1 K will be required to better investigate the potential SMM behavior. Nevertheless, the present work does establish interesting new examples of  $\text{Fe}_x$  clusters with significant ground-state  $S$  values and negative  $D$  values.

Finally, the preparation of complexes **1–4** again serves to emphasize the utility of alkoxide-containing chelates in polynuclear metal cluster chemistry, and the results of additional studies using new chelates related to  $\text{dmem}^-$  will be reported in due course.

**Acknowledgment.** We thank the National Science Foundation for support of this work.

**Supporting Information Available:** X-ray crystallographic data in CIF format for complexes **1**·4MeCN, **2**·MeCN, **3**·2MeCN, and **4**·CH<sub>2</sub>Cl<sub>2</sub> and two-dimensional contour plots of the fitting-error surface vs  $D$  and  $g$  for **1**· $\frac{1}{2}$ MeCN, **3**, and **4**· $\frac{1}{2}$ CH<sub>2</sub>Cl<sub>2</sub>. This material is available free of charge via the Internet at <http://pubs.acs.org>.

IC070106W